



Modular synthesis of amphiphilic chitosan derivatives based on copper-free click reaction for drug delivery

Yu Tao^{a,1}, Ding Qu^{a,b,1}, Chunli Tian^a, Yingshuang Huang^a, Lingjing Xue^a, Caoyun Ju^a, Meixi Hao^{a,*}, Can Zhang^{a,*}

^a State Key Laboratory of Natural Medicines, Jiangsu Key Laboratory of Drug Discovery for Metabolic Diseases, Center of Advanced Pharmaceuticals and Biomaterials, China Pharmaceutical University, Nanjing 210009, PR China

^b Affiliated Hospital of Integrated Traditional Chinese and Western Medicine, Nanjing University of Chinese Medicine, Nanjing 210028, PR China

ARTICLE INFO

Keywords:

Modular synthesis
Amphiphilic chitosan derivatives
SPAAC click reaction
Paclitaxel
Drug carrier

ABSTRACT

Amphiphilic chitosan derivatives have attracted wide attention as drug carriers due to their physicochemical properties. However, obtaining a desired amphiphilic chitosan derivative by tuning the various functional groups was complex and time-consuming. Therefore, a facile and common synthesis strategy would be promising. In this study, a modular strategy based on strain-promoted azide-alkyne cycloaddition (SPAAC) click reaction was designed and applied in synthesizing deoxycholic acid- or octanoic acid-modified *N*-azido propionyl-*N,O*-sulfate chitosan through tuning the hydrophobic groups. Additionally, chitosan derivatives with the same substitute groups were prepared via amide coupling as controls. We demonstrated that these derivatives via the two strategies showed no obvious difference in physicochemical properties, drug loading ability and biosafety, indicating the feasibility of modular strategy. Notably, the modular strategy exhibited advantages including high reactivity, flexibility and reproducibility. We believe that this modular strategy could provide varied chitosan derivatives in an easy and high-efficiency way for improving multifunctional drug carriers.

1. Introduction

Nanoparticle drug delivery systems (NDDSs) have shown promising benefits in disease therapy, including improved pharmacokinetic behavior, enhanced targeting ability, and reduced side effects (Guo et al., 2020). Despite NDDSs have achieved great progress over the past decades, the approved nano-formulations are still less than expected. As of the end of 2019, only a few nanomedicines have entered the clinical application stage (Anselmo and Mitragotri, 2019). One of the critical limitations that NDDSs faced is lacking enough multifunctional and safe biomaterials, which can protect chemotherapeutic agents from the complex physiological environment and *in vivo* barriers. Thus, the development of multifunctional and biocompatible drug vectors will be

beneficial to the advancement of NDDSs in the pharmaceutical industry (Becer et al., 2009).

Chitosan (CS), one of the most abundant natural polysaccharides obtained from *N*-deacetylation of chitin (Ali and Ahmed, 2018), has attracted increasing attentions in the field of drug delivery and as antibacterial and antifungal agents by virtue of its unique biocompatibility and biodegradability. Notably, the abundant amino and hydroxyl groups provide chitosan with an excellent chemical modifiability and function expandability. For example, sulfonation of chitosan has been widely investigated, which significantly improves the solubility of chitosan (Dimassi et al., 2018) and endows the outstanding bioactivities such as antioxidant (Seedeve et al., 2017) and anticoagulant (Campelo et al., 2016). Besides, amphiphilic chitosan derivatives equipping with

Abbreviations: NDDSs, nanoparticle drug delivery systems; CS, chitosan; SC, *N,O*-sulfate chitosan; ASC, *N*-azido propionyl-*N,O*-sulfate chitosan; ADIBO, azadibenzocyclooctyne; ADIBO-DOC, ADIBO-modified deoxycholic acid; ADIBO-Oct, ADIBO-modified octanoic acid; SPAAC, strain-promoted azide-alkyne cycloaddition; DCSC, deoxycholic acid-modified *N*-azido propionyl-*N,O*-sulfate chitosan; OCSC, octanoic acid-modified *N*-azido propionyl-*N,O*-sulfate chitosan; DSC, deoxycholic acid-modified *N,O*-sulfate chitosan; OSC, octanoic acid-modified *N,O*-sulfate chitosan; PTX, paclitaxel; PTX-DCM, PTX-loaded DCSC micelles; PTX-OCM, PTX-loaded OCSC micelles; PTX-DM, PTX-loaded DSC micelles; PTX-OM, PTX-loaded OSC micelles.

* Corresponding authors at: State Key Laboratory of Natural Medicines, Jiangsu Key Laboratory of Drug Discovery for Metabolic Diseases, Center of Advanced Pharmaceuticals and Biomaterials, China Pharmaceutical University, Nanjing, PR China.

E-mail addresses: haomeixi@cpu.edu.cn (M. Hao), zhangcan@cpu.edu.cn (C. Zhang).

¹ Authors contributed equally to this work.

<https://doi.org/10.1016/j.ijpharm.2021.120798>

Received 26 April 2021; Received in revised form 7 June 2021; Accepted 9 June 2021

Available online 12 June 2021

0378-5173/© 2021 Elsevier B.V. All rights reserved.

various hydrophobic and hydrophilic groups have been extensively studied as functional drug carriers (Di Martino and Sedlarik, 2014). During the last decade, our group has designed and synthesized a series of amphiphilic chitosan derivatives, such as *N*-octyl-*O*-sulfate chitosan (NOSC) (Jin et al., 2014; Mo et al., 2011), *N*-octyl-*N*,*O*-succinyl-*O*-phosphoryl chitosan (OSPC) (Zhang et al., 2016), *N*-octyl-*N'*-phthalyl-*O*-phosphate chitosan (OPPC) (Qu et al., 2020), and so on, which could self-assemble into micelles for effective drug delivery and enhanced anticancer treatment. However, conventional synthesis of amphiphilic chitosan derivatives has to choose a certain reaction technology according to the characteristics of the modified segments, such as *N*-acylation (Lai et al., 2017), reductive amination (de Oliveira Pedro et al., 2016; Gabriel et al., 2017), *N*-alkylation (Wakita, 2013) and *O*-carboxymethylation (Du et al., 2014). Such varied modifications bring complexity and time-consuming to the extensive synthesis of various amphiphilic chitosan derivatives. Therefore, a facile and common synthetic strategy is urgently required to address the issues mentioned above.

“Click” chemistry has been widely used in bioconjugation, which allows for desired biomolecules joining to the substrate (Zou et al., 2018). However, the previous click chemistry is commonly involved with copper-containing organics, which are not only unfriendly to the environment but also brings many obstacles to *in vivo* applications. Recently, a strain-promoted azide-alkyne cycloaddition (SPAAC) has been reported through a reaction between aza-dibenzocyclooctyne (ADIBO) and azido groups, showing promising potential in chitosan-based modifications due to high reactivity, simple post-processing, and purification but no need for copper-containing catalysis (Smyslova et al., 2015). With all these advantages, SPAAC has shown promising potential in chitosan-based modifications like protein conjugation and radiolabeling (Jung and Yi, 2013; Lee et al., 2013). Therefore, we would employ SPAAC to synthesize amphiphilic chitosan derivatives in a safe and effective way, which is also expected to facilitate adjust the ratio between hydrophobic and hydrophilic groups according to needs.

Herein, we described a SPAAC-based modular strategy to verify the significance of our idea (Fig. 1 and Fig. 2). First, *N*,*O*-sulfate chitosan (SC) was synthesized by sulfonation to improve the solubility of chitosan for the convenience of further modification. Azido groups were then introduced into the chitosan backbone through amide coupling to gain *N*-azido propionyl-*N*,*O*-sulfate chitosan (ASC) for the following click reaction (Fig. 2A). Next, two hydrophobic groups including ADIBO-modified deoxycholic acid and octanoic acid (ADIBO-DOC and ADIBO-Oct) were synthesized as the hydrophobic modules for click reaction (Fig. 2B). Finally, ASC reacted with ADIBO-DOC or ADIBO-Oct via SPAAC under gentle condition to facilitate afford amphiphilic chitosan derivatives deoxycholic acid-modified *N*-azido propionyl-*N*,*O*-sulfate chitosan (DCSC) and octanoic acid-modified *N*-azido propionyl-*N*,*O*-sulfate chitosan (OCSC) (Fig. 2C). To evaluate the feasibility of modular synthesis strategy, amphiphilic chitosan derivatives *N*-deoxycholoyl-*O*-sulfate chitosan (DSC) and *N*-octyl-*O*-sulfate chitosan (OSC) with the same hydrophilic and hydrophobic groups were synthesized through the direct amide coupling method as controls (Fig. 2D). The four amphiphilic chitosan derivatives were confirmed by ^1H nuclear magnetic resonance (^1H NMR), Fourier transform infrared spectrometer (FT-IR), and elemental analysis, respectively. The critical micelle concentration (CMC) of different derivatives was detected using the pyrene fluorescence method to evaluate their self-assembly ability. Additionally, amphiphilic chitosan derivatives were served as drug carriers to encapsulate paclitaxel (PTX), a kind of mitotic inhibitor with good antitumor activity but poor water solubility. Subsequently, PTX-loaded micelles were systematically investigated in terms of loading capability, *in vitro* stability, drug release behavior, as well as antitumor ability. The obtained results showed no obvious difference in physicochemical properties of amphiphilic chitosan derivatives between distinct synthesis strategies, while the SPAAC-based modular strategy presented higher reactivity and yield but no inoffensive byproducts.

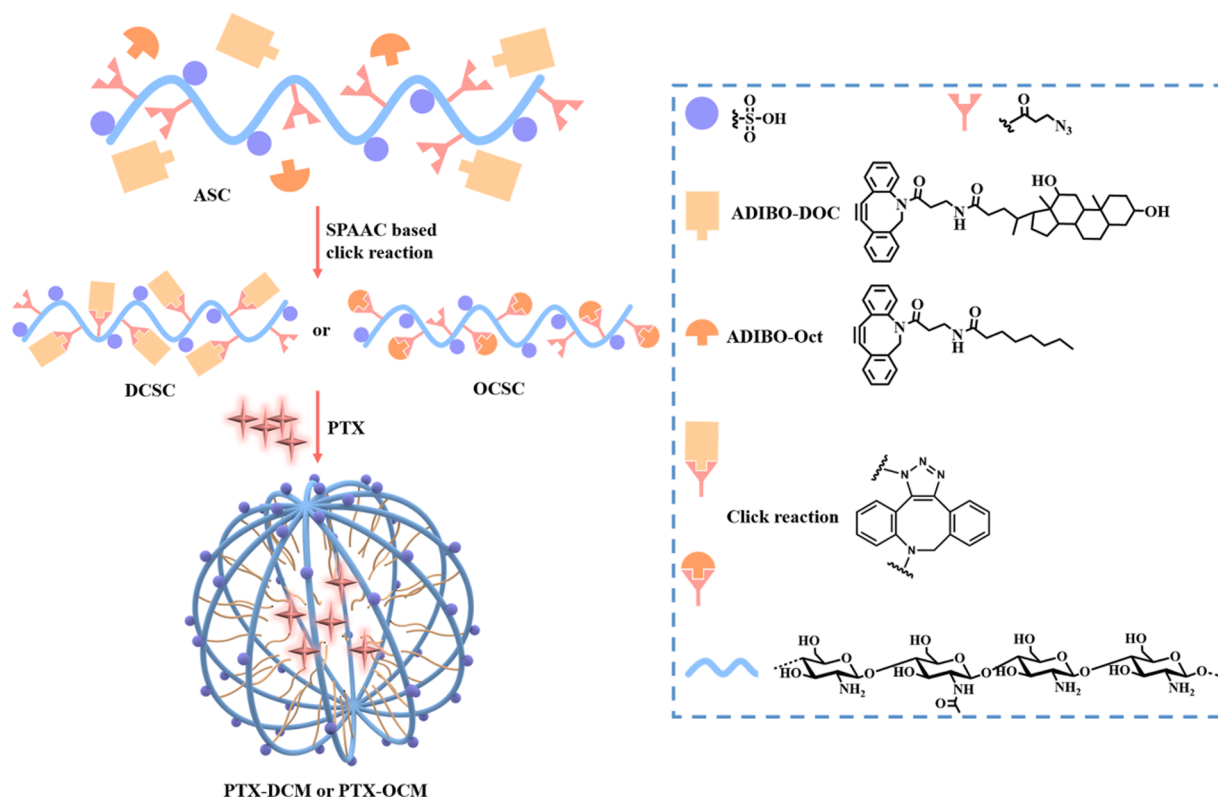


Fig. 1. Schematic representation for modular synthesis of DCSC and OCSC based on SPAAC reaction. The two amphiphilic chitosan derivatives can self-assemble into micelles and stably encapsulate PTX in the hydrophobic core.

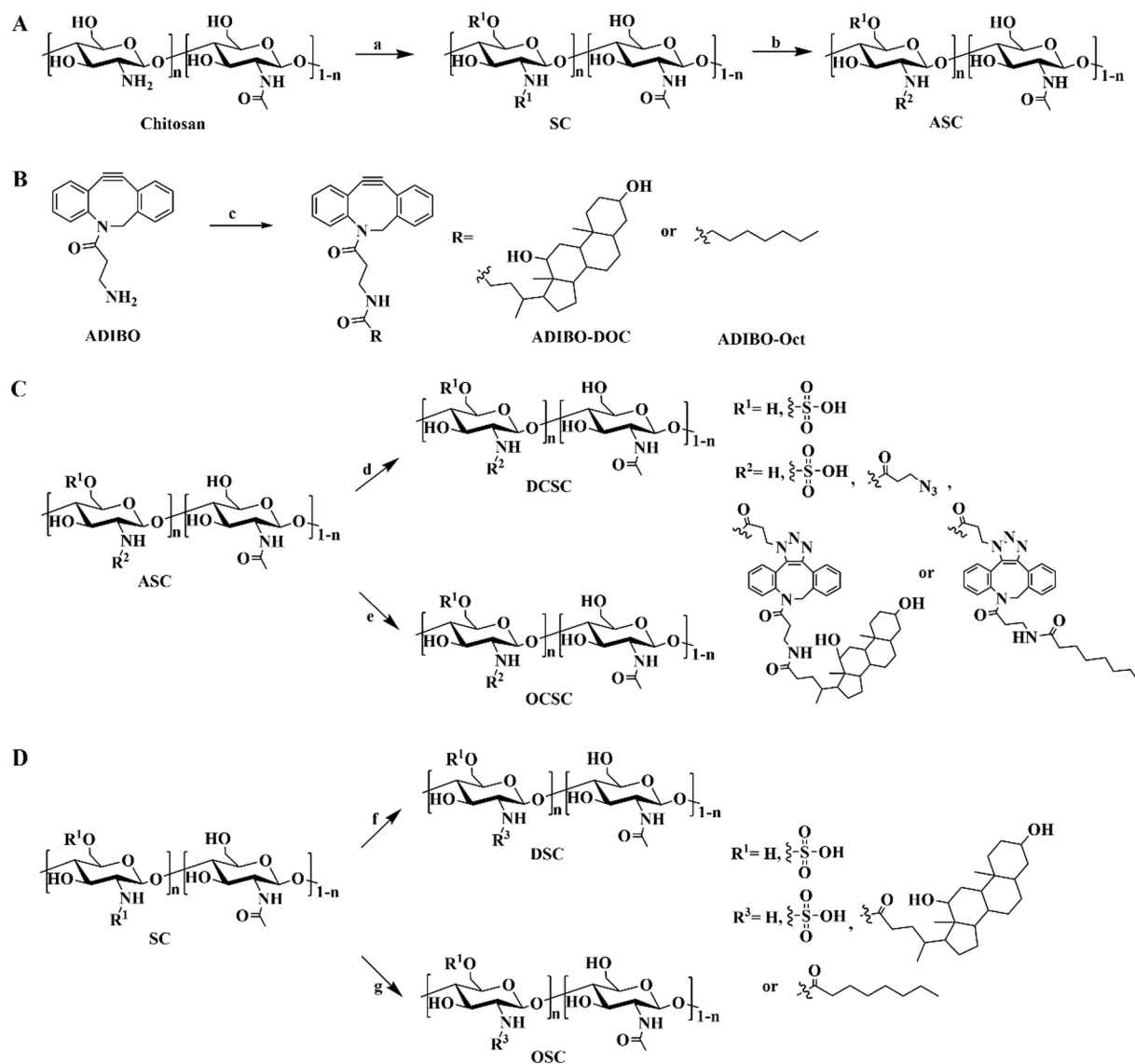


Fig. 2. Synthetic routes of chitosan derivatives. (A) Synthesis of ASC. (B) Synthesis of ADIBO-DOC and ADIBO-Oct. (C) Synthesis of DCSC and OCSC based on SPAAC reaction. (D) Synthesis of DSC and OSC based on amide condensation.

2. Experimental

2.1. Materials

Chitosan was purchased from Zhejiang Golden Shell Pharmaceutical Co., Ltd. (Zhejiang, China), with a deacetylation degree of 84% and viscosity average molecular weight of 50 kDa. PTX was obtained from Yew Pharmaceutical Co., Ltd. (Jiangsu, China). Taxol® was purchased from Shanghai Squibb Pharmaceutical Co., Ltd. Deoxycholic acid, octanoic acid and coumarin 6 (C6) were purchased from Aladdin Reagent Inc. (Shanghai, China). Fetal bovine serum (FBS), Dulbecco's modified Eagle's medium (DMEM), and 3-(4,5-dimethylthiazol-2-yl)-2,5-diphenyltetrazolium bromide (MTT) were purchased from Thermo Fisher Scientific Inc. All other chemicals and reagents were analytical grade and obtained from Aladdin Reagent Inc. (Shanghai, China).

2.2. Modular synthesis of DCSC and OCSC

2.2.1. Preparation of ASC

Hydrophilic module ASC was synthesized as shown in Fig. 2A. CS (5.00 g, 30.70 mmol of glucosamine) was dispersed in the mixture of

formamide (200 mL) and formic acid (6 mL), followed by stirring at room temperature for 6 h. Chlorosulfonic acid (10.00 mL, 153.50 mmol) was added dropwise into *N,N*-dimethylformamide (DMF, 100 mL) at 0 °C under a nitrogen atmosphere and stirred for 1 h. After being heated to room temperature and stirred for another 30 min, the chlorosulfonic acid solution was mixed with chitosan and reacted at 45 °C under nitrogen atmosphere for 2 h. The solution was adjusted to pH 7 with 40% (w/v) NaOH, followed by filtration. The filtrate was dialyzed using a dialysis bag (molecular weight cut-off range, MWCO, 8–14 kDa) against deionized water for 3 days, followed by freeze-drying to gain SC (2.20 g, 44.0%) as a yellow solid.

3-azido propionic acid (1.20 g, 10.43 mmol), 1-ethyl-3-(3-dimethylaminopropyl) carbodiimide hydrochloride (EDCI, 3.00 g, 15.64 mmol) and *N*-hydroxysuccinimide (NHS, 1.26 g, 10.94 mmol) were stirred in H₂O (20 mL) at room temperature for 2 h, followed by the addition of SC (0.85 g, 5.21 mmol) dissolved in H₂O (20 mL). The resulting mixture was stirred at room temperature for 24 h and dialyzed (MWCO 8–14 kDa) against deionized water for 3 days, followed by freeze-drying to give ASC (0.65 g, 70.0%) as a yellow solid.

2.2.2. Synthesis of ADIBO-DOC and ADIBO-Oct

ADIBO, a hydrophobic module, was synthesized according to the previous report (Kuzmin et al., 2010). The detailed synthetic methods are introduced in Fig. S1 and Supplementary Methods.

Hydrophobic modules ADIBO-DOC and ADIBO-Oct were prepared following Fig. 2B. ADIBO (0.94 g, 3.40 mmol) and triethylamine (TEA, 1.50 mL, 10.19 mmol) were dissolved in CHCl_3 (20 mL) at room temperature, followed by the addition of the DMF solution of deoxycholic acid (1.60 g, 4.08 mmol) or octanoic acid (0.59 g, 4.08 mmol), EDCI (0.85 g, 4.42 mmol) and NHS (0.51 g, 4.42 mmol). After reaction for 12 h, the suspension was diluted with CH_2Cl_2 , rinsed with water and 10% citric acid successively, and dried by anhydrous Na_2SO_4 . The solvent was removed to afford the crude product, followed by purifying by column chromatography on silica gel eluted with ($\text{CH}_2\text{Cl}_2/\text{MeOH}$, 30:1) to obtain yellow powdered ADIBO-DOC (1.80 g, 81.8%), or with ($\text{CH}_2\text{Cl}_2/\text{MeOH}$, 25:1) to gain yellow solid ADIBO-Oct (1.10 g, 76.9%). The ^1H NMR, ^{13}C NMR, high resolution mass spectrum (HRMS) spectra of ADIBO-DOC and ADIBO-Oct were shown in Fig. S2 and S3.

2.2.3. Synthesis of DCSC and OCSC

As illustrated in Fig. 2C, amphiphilic derivatives DCSC and OCSC were prepared via click reaction. ADIBO-DOC (0.16 g, 0.24 mmol) or ADIBO-Oct (0.05 g, 0.12 mmol) was dissolved in dimethyl sulfoxide (DMSO, 4 mL) with an addition of ASC (0.20 g, 1.23 mmol) aqueous solution at 30 °C under stirring. The resulting mixture was stirred at room temperature for 24 h, dialyzed (MWCO 8–14 kDa) against DMSO for 2 days and then against deionized water for 3 days successively. After freeze-drying, DCSC (0.33 g, 92.0%) or OCSC (0.23 g, 90.0%) was obtained as a yellow solid.

2.3. Direct synthesis of DSC and OSC

DSC and OSC were prepared as shown in Fig. 2D. Deoxycholic acid (1.60 g, 4.08 mmol) or octanoic acid (0.59 g, 4.08 mmol), EDCI (0.85 g, 4.42 mmol) and NHS (0.51 g, 4.42 mmol) were stirred in DMSO (20 mL) at room temperature for 2 h, followed by the addition of SC (0.44 g, 2.72 mmol) aqueous solution. The mixture was stirred at 30 °C for 24 h, dialyzed (MWCO 8–14 kDa) against DMSO for 2 days and then against deionized water for 3 days successively. After freeze-drying, yellow solid DSC (0.30 g, 68.0%) or OSC (0.29 g, 64.0%) was obtained.

2.4. Characterization of chitosan derivatives

The chemical structures of DCSC, DSC, OCSC and OSC were confirmed by ^1H NMR spectra collected on a Bruker AVANCE-300 spectrometer (Switzerland, provided by Bruker Tech. and Serv. Co., Ltd. Beijing, China), with 99.9% deuterium oxide (D_2O) as the solvent. The successful introduction of diverse groups into the backbone of chitosan was identified by FT-IR spectra, which were recorded with KBr pellets on a TENSOR 27 spectrometer (Bruker, Karlsruhe, Germany). The C, H, and N proportions in synthesized products were determined by an Element Vario EL III analyzer (Elementar, Germany). The substitution degree (DS) of chitosan derivative was defined as the molar number of conjugated groups per mol of monomeric unit of chitosan and calculated according to the following formula (dos Santos et al., 2009): $W = (M_C \times n_{\text{CD}} \times n_{\text{D}} + M_C \times n_{\text{CA}} \times n_{\text{A}}) / (M_N \times n_{\text{ND}} \times n_{\text{D}} + M_N \times n_{\text{NA}} \times n_{\text{A}})$, where W represents the mass ratio between carbon and nitrogen in chitosan derivatives; M_C and M_N are the molar mass of carbon and nitrogen, $M_C = 12$, $M_N = 14$; n_{CD} and n_{ND} are the number of carbon and nitrogen moles per mole of deacetylated unit; n_{CA} and n_{NA} is the number of carbon and nitrogen moles per mole of acetylated unit; n_{D} is the number of moles of deacetylated units in chitosan derivatives, n_{A} is the number of moles of acetylated units in chitosan derivatives. The results of elemental analysis and detailed calculation processes are shown in Supplementary Methods.

2.5. Physicochemical properties of chitosan derivatives

2.5.1. Molecular weight

The molecular weight of DCSC, DSC, OCSC or OSC was determined via viscosity (η) determination with an Ubbelohde capillary viscometer at 25 °C (Sun et al., 2007). Chitosan derivatives were respectively dissolved in 0.1 M NaCl and diluted to various concentrations (0.5, 1.0, 2.0, 3.0 and 5.0 mg/mL). The molecular weight (M_w) was calculated referring to the following formula: $\eta = KM^\alpha$, where $K = 0.00181 \text{ cm}^{-3}/\text{g}$, $\alpha = 0.93$.

2.5.2. Water solubility

0.1 g of DCSC was stirred in deionized water (10 mL) at 25 °C for 5 h to give a saturated solution with insoluble remains. The undissolved solid was then collected by gravity filtration, washed with acetone and dried at 40 °C under vacuum overnight. The solubility (S) was calculated according to the following equation: $S (\text{g}) = (0.1 - W_1) / 0.1 \times 100$, where $W_1(\text{g})$ is the weight of undissolved polymers. Likewise, the water solubility of DSC, OCSC or OSC was determined by the same method.

2.5.3. Critical micelle concentration (CMC)

The self-aggregation characteristic of DCSC was evaluated by fluorescence spectroscopy using pyrene as a probe (Yu et al., 2017). A serial dilution of polymer in aqueous solution was prepared at various concentrations ranging from 1×10^{-4} mg/mL to 1 mg/mL. 100 μL of pyrene (7×10^{-5} M in acetone) was prepared, followed by evaporation of organic solvent at room temperature overnight. Subsequently, pyrene was added into the above derivative solution. Then the mixture was sonicated for 30 min and incubated at 65 °C for 3 h. After being cooled to room temperature and left standing overnight, the emission spectra (330–550 nm) of the solutions were recorded at an excitation wavelength of 335 nm using an RF-5301 PC fluorescence spectrophotometer (Shimadzu, Kyoto, Japan). Peak height intensity ratio (I_1/I_3) of the first peak (I_1 at 373 nm) to the third peak (I_3 at 384 nm) was plotted against the logarithm of polymer concentration. The CMC value was taken from the intersection point of two tangents along the curve. Similarly, the CMC value of DSC, OCSC or OSC was estimated by the same method.

2.6. Preparation and characterization of PTX-loaded micelles

PTX-loaded micelles were prepared by the dialysis method described previously with slight modification (Jin et al., 2014). In brief, PTX (10 mg) dissolved in ethanol (222 μL) was added into the aqueous solution of DCSC, OCSC, DSC or OSC (10 mg) under vigorous stirring. The resulting mixture was dialyzed (MWCO 8–14 kDa) against deionized water at room temperature for 12 h and filtrated through 0.22 μm membrane to afford PTX-loaded DCSC micelles (PTX-DCM), PTX-loaded OCSC micelles (PTX-OCM), PTX-loaded DSC micelles (PTX-DM) or PTX-loaded OSC micelles (PTX-OM).

The content of PTX in the micelles was determined by high performance liquid chromatography (HPLC) (Shimadzu, Kyoto, Japan). The encapsulation efficiency (EE%) and drug loading capacity (LC%) were calculated according to the following equations: $EE (\%) = W_{\text{PTX}} / W_t \times 100$; $LC (\%) = W_{\text{PTX}} / (W_{\text{PTX}} + W_{\text{ACD}}) \times 100$, where W_{PTX} , W_t and W_{ACD} were the quantities of PTX encapsulated in the micelles, the feeding PTX and chitosan derivatives in the micelles, respectively.

The particle sizes and zeta potentials of micelles were measured by dynamic light scattering (DLS) (Zetasizer 3000 HAS, Malvern, UK) at 25 °C. The morphology of micelles was investigated using transmission electron microscopy (TEM) on a JEM-200CX electron microscope (JEOL, Japan) at 80 kV. Sample solution was dropped on the copper grid, stained with 1% (v/v) sodium phosphotungstate aqueous solution and air-dried before observation, successively.

2.7. *In vitro* stability of PTX-loaded micelles

The *in vitro* stability of PTX-loaded micelles included storage stability and plasma stability. In brief, the storage stability was investigated by the assessment of PTX leakage from micelles and the size change of micelles stored at 4 °C for 7 days. The particle sizes and LC (%) of various PTX-loaded micelles were detected every day using DLS and HPLC, respectively. Moreover, the size change of PTX-loaded micelles under mimic physiological conditions including phosphate buffer (PB, 20 mM, pH 7.4) and DMEM containing 10% FBS at 37 °C were recorded at predetermined time to evaluate the plasma stability, respectively.

2.8. Drug release of PTX-loaded micelles

In vitro drug release was evaluated by a dialysis method. Briefly, 0.5 mL PTX-loaded micelles (0.5 mg PTX) in a dialysis bag (MWCO 8–14 kDa) were immersed in different buffer solution (40 mL) with stirring at 100 rpm under 37 °C. The release media included PB (20 mM, pH 7.4) and acetate buffer (20 mM, pH 5.5), respectively. PB buffer (pH 7.4) is prepared by mixture of 19 mL NaH₂PO₄ (20 mM) and 81 mL Na₂HPO₄ (20 mM), while acetate buffer (pH 5.5) is prepared by mixture of 90 mL CH₃COONa (20 mM) and 10 mL CH₃COOH (20 mM). They both contained 0.1% (w/v) Tween 80 to keep in accordance with a sink condition. At predetermined time intervals (0.5 ~ 60 h), 1 mL of buffer solution was withdrawn for HPLC analysis and replaced with fresh medium.

2.9. Cell culture

Human breast cancer (MCF-7) cells and human umbilical vein endothelial (HUVEC) cells were purchased from the Cell Bank of Chinese Academy of Sciences (Shanghai, China). The cells were maintained in the DMEM supplemented with 10% (v/v) FBS and 1% penicillin–streptomycin in an incubator (Thermo Fisher Scientific Inc., USA) at 37 °C under an atmosphere of 5% CO₂ and 90% relative humidity.

2.10. Cytotoxicity of chitosan derivatives against HUVEC cells

HUVEC cells were seeded in 96-well plates at a density of 5×10^4 cells per well and incubated for 24 h. The medium was then removed and cells were treated with diversified chitosan derivatives at a final concentration from 10 to 500 µg/mL for 72 h. Afterwards, 20 µL of MTT PBS solution (5 mg/mL) was added into each well for a further 4 h incubation. Then the supernatant was eliminated carefully and DMSO (150 µL) was added to dissolve formazan crystals. The absorbance of the solution was measured at 570 nm by a microplate reader (BioTek Instruments, USA). The relative cell viability was calculated as follows: relative cell viability (%) = absorbance of the treated cells/absorbance of the untreated cells × 100.

2.11. Cellular uptake of C6-loaded micelles

Confocal laser scanning microscope (CLSM) and flow cytometry were both employed to estimate MCF-7 cellular uptake of various micelles. C6-loaded micelles (C6-DCM, C6-DM and C6-OCM) were prepared by the procedure for PTX-loaded micelles except by replacing PTX with C6 (6 µg/mL). MCF-7 cells were seeded in laser confocal dish at a density of 1×10^5 cells per well and incubated for 24 h. After removal of culture medium, MCF-7 cells were incubated with C6-loaded micelles (200 µL). At predetermined time (0.5 h, 1 h, 2 h, 4 h and 6 h), cells were rinsed with ice-cold PBS thrice and fixed with 4% paraformaldehyde for 30 min. After that, the cells were stained by Hoechst 33,342 for 15 min and washed with ice-cold PBS thrice, followed by the observation using a CLSM (Zeiss LSM 880, Germany).

For flow cytometry, MCF-7 cells were seeded in 24-well plates at a density of 4×10^5 cells per well and incubated for 24 h. After removal of

culture medium, MCF-7 cells were incubated with C6-loaded micelles. The cells were then rinsed with ice-cold PBS thrice and detached by 0.025% trypsin/ethylenediaminetetraacetic acid (EDTA), followed by centrifugation at 1000 rpm for 5 min. Eventually, cells were resuspended in PBS and analyzed utilizing a BD Accuri™ C6 Plus flow cytometer (Becton Dickinson, San Jose, CA).

2.12. Cytotoxicity of PTX-loaded micelles against MCF-7 cells

MCF-7 cells were seeded in 96-well plates at a density of 5×10^3 cells per well and incubated for 24 h. After removal of culture medium, the cells were respectively treated with various PTX-loaded micelles at the PTX concentrations ranging from 0.05 to 20 µg/mL for 48 h, and Taxol was used as a positive control. Afterwards, 20 µL of MTT solution (5 mg/mL) was added into each well for a further 4 h-incubation. Afterwards, the supernatant was removed carefully and DMSO (150 µL) was added to dissolve formazan crystals. The absorbance of the solution was measured at 570 nm using a Tecan microplate reader. The half maximal inhibitory concentration (IC₅₀) was calculated using nonlinear regression analysis.

2.13. Statistical analysis

All data were presented as the mean value with standard deviation (SD) of at least triplicate measurements. Statistical analyses were tested using a two-tailed Student's *t*-test or one-way ANOVA. Statistical significance was set at **P* < 0.05, and extreme significance was set at ***P* < 0.01 (GraphPad Prism 8.0.1).

3. Results

3.1. Synthesis and characterizations of chitosan derivatives

We have successfully synthesized two amphiphilic chitosan derivatives via modular synthesis strategy based on SPAAC click reaction between azide groups on chitosan backbone and different hydrophobic modules (ADIBO-DOC or ADIBO-Oct). The ratio of hydrophobic segments in amphiphilic chitosan derivatives closely relates to the drug entrapment (Kim et al., 2001). To optimize the drug entrapment efficiency of DCSC and OCSC, the best molar ratio of ADIBO-DOC and ADIBO-Oct to ASC was screened. Since the DS of azidopropionyl in ASC was 0.18, the equivalents between ADIBO-DOC/ADIBO-Oct and ASC were set as 0.05:1, 0.1:1, 0.2:1, respectively (Table S1). It turned out that the best equivalent for ADIBO-DOC and ADIBO-Oct was 0.2:1 and 0.1:1. Due to the fixed equivalent, the DS of DOC or Oct reached a maximum of 0.13 and 0.15, respectively. In addition, DSC and OSC were also synthesized on the basis of direct *N*-deoxycholoylation or *N*-octanoylation. To evaluate the influence of synthetic methods on drug entrapment, the molar ratio of deoxycholic acid and octanoic acid of DSC and OSC was controlled to achieve a similar level with that of DS of DCSC and OCSC (Table 1).

¹H NMR spectra and FT-IR were performed to confirm the chemical structure of these chitosan derivatives (Fig. 3A and B). As for DCSC and DSC, the intensive signals at δ1.09 and 1.25 ppm were probably attributed to deoxycholyl groups. One broad peak in the ranges of δ3.60 to 4.36 ppm might be ascribed to the protons of *N*-acetyl glucosamine and glucosamine units. The peak at δ2.04 ppm could be assigned to the methyl protons of *N*-acetyl groups (Qu et al., 2013; Wu et al., 2016). Of note, the peaks newly-appeared at δ8.03 and δ8.25 ppm were attributed to the aromatic ring of ADIBO (Kuzmin et al., 2010). These peaks indicate the conjugation of ADIBO-DOC with ASC through Huisgen 1,3-dipolar cycloaddition between azides and alkynes. Similarly, the prominent signal was observed at δ0.86 and δ1.27 ppm in both ¹H NMR spectra of OCSC and OSC, which might be ascribed to octanoyl groups (Qu et al., 2020). Likewise, the new signal appeared at δ8.02 and δ8.23 ppm was corresponding to the aromatic ring of ADIBO, suggesting that

Table 1Characterizations and physicochemical properties of different chitosan derivatives ($n = 3$).

Compound	Equivalents ^a (mol:mol)	DS ^b	Yield (%)	M_n	Solubility (g/L)	CMC ($\mu\text{g}/\text{mL}$)
CS	N/A	N/A	N/A	50,000	0.005	N/A
DCSC	0.2:1	0.13	92.0 \pm 1.3 ^{**}	34,425	8.4	50.3
DSC	1.5:1	0.15	68.0 \pm 5.5	42,434	9.1	10.4
OCSC	0.1:1	0.10	90.0 \pm 2.0 ^{**}	45,020	6.5	8.3
OSC	1.5:1	0.10	64.0 \pm 6.2	42,973	10.7	21.5

^a For DCSC and OCSC, the equivalents mean the molar ratio between ADIBO-DOC/ADIBO-Oct and monomeric units of ASC; for DSC and OSC, the equivalents mean the molar ratio between deoxycholic acid/octanoic acid and monomeric units of SC.

^b For DCSC and DSC, the DS means the molar number of grafted deoxycholoyl groups per mol of monomeric units of chitosan; for OCSC and OSC, the DS means the molar number of grafted octyl groups per mol of monomeric units of chitosan.

** $P < 0.01$.

OCSC was successfully synthesized via the conjugation of ADIBO-Oct with ASC based on SPAAC click reaction.

As depicted in Fig. 3B, the FT-IR characteristic absorbance peaks at 3415, 1065 cm^{-1} were observed, which were ascribed to the stretching vibration of $-\text{NH}_2$, $-\text{OH}$ on the chitosan backbone and the stretching vibration of C—O bond on the glucosamine ring, respectively. The new peaks at 2115 cm^{-1} belonged to residual azide groups of DCSC and OCSC (Wang et al., 2017), indicating the existence of azido propionyl groups on chitosan backbone. Notably, the signal around 1560 cm^{-1}

could be assigned to the characteristic absorbance of 1,2,3-triazole ring (Hashidzume et al., 2013), further verifying the conjugation between hydrophobic and hydrophilic module via SPAAC click reaction.

Moreover, the yields of DCSC and OCSC were both beyond 90%, which was remarkably improved compared to that of DSC and OSC (Table 1). Such modular synthesis not only presents the yield superiority but also reduces batch-to-batch variation. Importantly, no obvious difference was found in viscosity-average molecular weight (M_n), water solubility, and CMC resulted from two synthetic methods, indicating that modular synthesis is promising as a supplementary method in developing amphiphilic chitosan derivatives. Of note, the introduction of ADIBO groups significantly increased the hydrophobicity for chitosan derivatives, which is helpful to improve its drug loading capacity.

3.2. Preparation and characterization of PTX-loaded micelles

PTX, a broad-spectrum hydrophobic chemotherapeutic agent (Davis et al., 2008), was applied as an encapsulated drug to evaluate the drug loading ability of amphiphilic chitosan derivatives. Following the previously reported methods (Jin et al., 2014), DCSC, DSC and OCSC self-assemble into micelles to encapsulate hydrophobic PTX into their inner cavity by dialysis method, respectively. Unlike the other three vectors, OSC lacked sufficient capacity to load PTX, probably due to the insufficient matching between hydrophobic units and PTX (Table 1). In contrast, OCSC shared a similar substitution degree of hydrophobic groups with OSC but was capable of encapsulating PTX because of the introduction of ADIBO as a linker. In view of this, PTX-loaded OSC micelles (PTX-OM) would not be studied in the following parts.

The other three PTX-loaded micelles including PTX-loaded DCSC micelles (PTX-DCM), PTX-loaded DSC micelles (PTX-DM), and PTX-loaded OCSC micelles (PTX-OCM) showed similar particle sizes of ~ 150 nm and zeta potentials around -18 mV (Table 2), with uniformly spherical nanostructure as observed in TEM and SEM images (Fig. 4A and Fig. S4). Of note, the average particle size of PTX-DCM was smaller

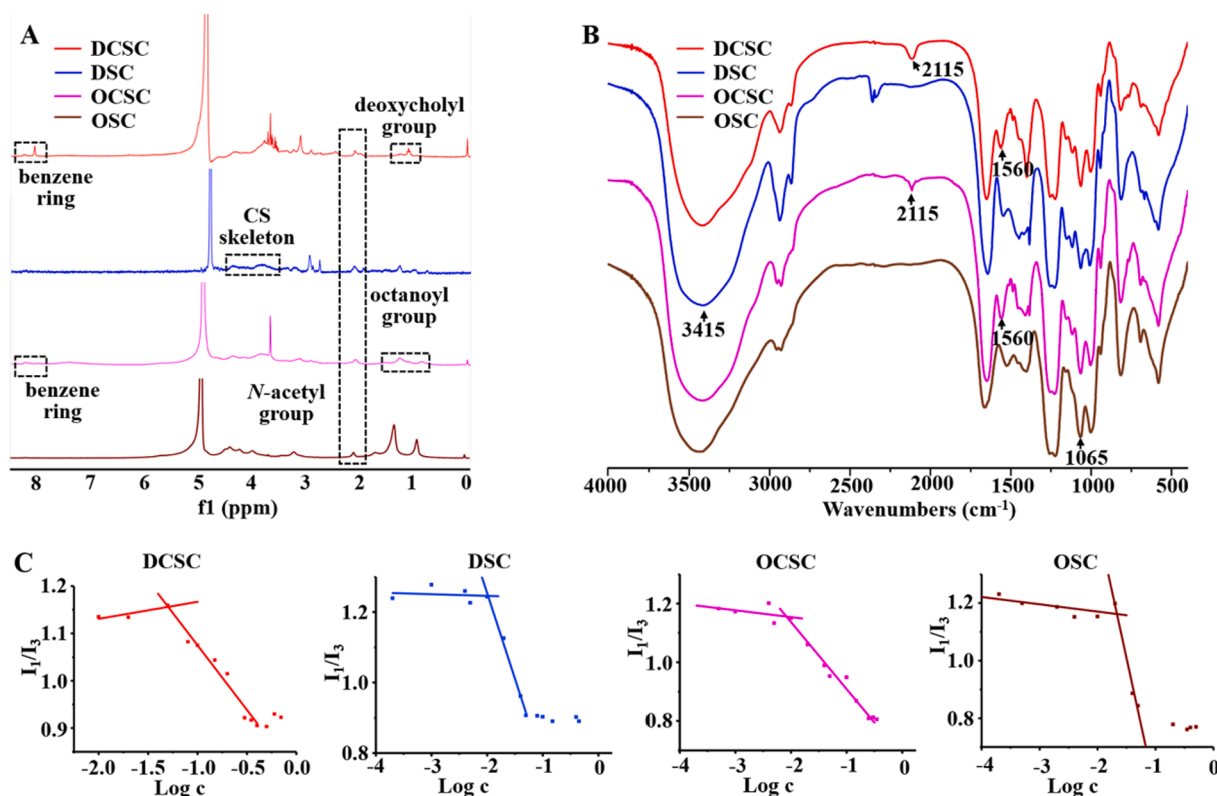


Fig. 3. Characterizations of chitosan derivatives. (A) ^1H NMR spectra. (B) FT-IR spectra. (C) Determination of CMC.

Table 2
Characterizations of various PTX-loaded micelles (n = 3).

Formulation	Size (nm)	PDI	Zeta potential (mV)	EE (%)	LC (%)
PTX-DCM	145.1 ± 3.1	0.1 ± 0.07	-18.9 ± 0.7	82.8 ± 1.4	44.3 ± 1.4
	155.4 ± 2.0	0.05 ± 0.06	-21.7 ± 1.8	63.3 ± 1.1	37.9 ± 1.2
PTX-DM	158.2 ± 2.6	0.1 ± 0.06	-15.2 ± 1.4	65.8 ± 1.6	39.3 ± 1.4

than that of PTX-DM, which was due to the more compact core resulted from the extra hydrophobicity of ADIBO. The above-mentioned result was also in accordance with the TEM images. Moreover, the particle sizes of DCM, DM and OCM micelles without drug loading were about 120 nm with uniformly spherical nanostructure (Table S2 and Fig. S5), which were generally smaller than that of PTX-loaded micelles, further

indicating the successful encapsulation of PTX in hydrophobic core. The negative charge of drug-loaded micelles was associated with the numerous sulfonfyl groups, which assisted to improve the *in vivo* stability and biosafety. Table 2 listed the drug encapsulation efficiency and loading efficiency of various micelles. Each micelle possessed a PTX loading capacity of around 40%, thereinto, PTX-DCM exhibited overwhelming encapsulation efficiency among all the groups.

Additionally, the storage and simulated *in vivo* stability of PTX-loaded micelles were evaluated by HPLC and DLS, respectively. As shown in Fig. 4B and 4C, all three micelles maintained structural integrity with a low drug leakage (<15%) in deionized water at 4 °C within 7 days. Although the particle size increased slightly because of non-specific binding with protein, the micelles were stable in PB of pH 7.4 and DMEM containing 10% FBS at 37 °C within 12 h (Fig. 4D). These results indicated that the stability of these micelles was acceptable under storage and physiological conditions, which meet the basic requirements

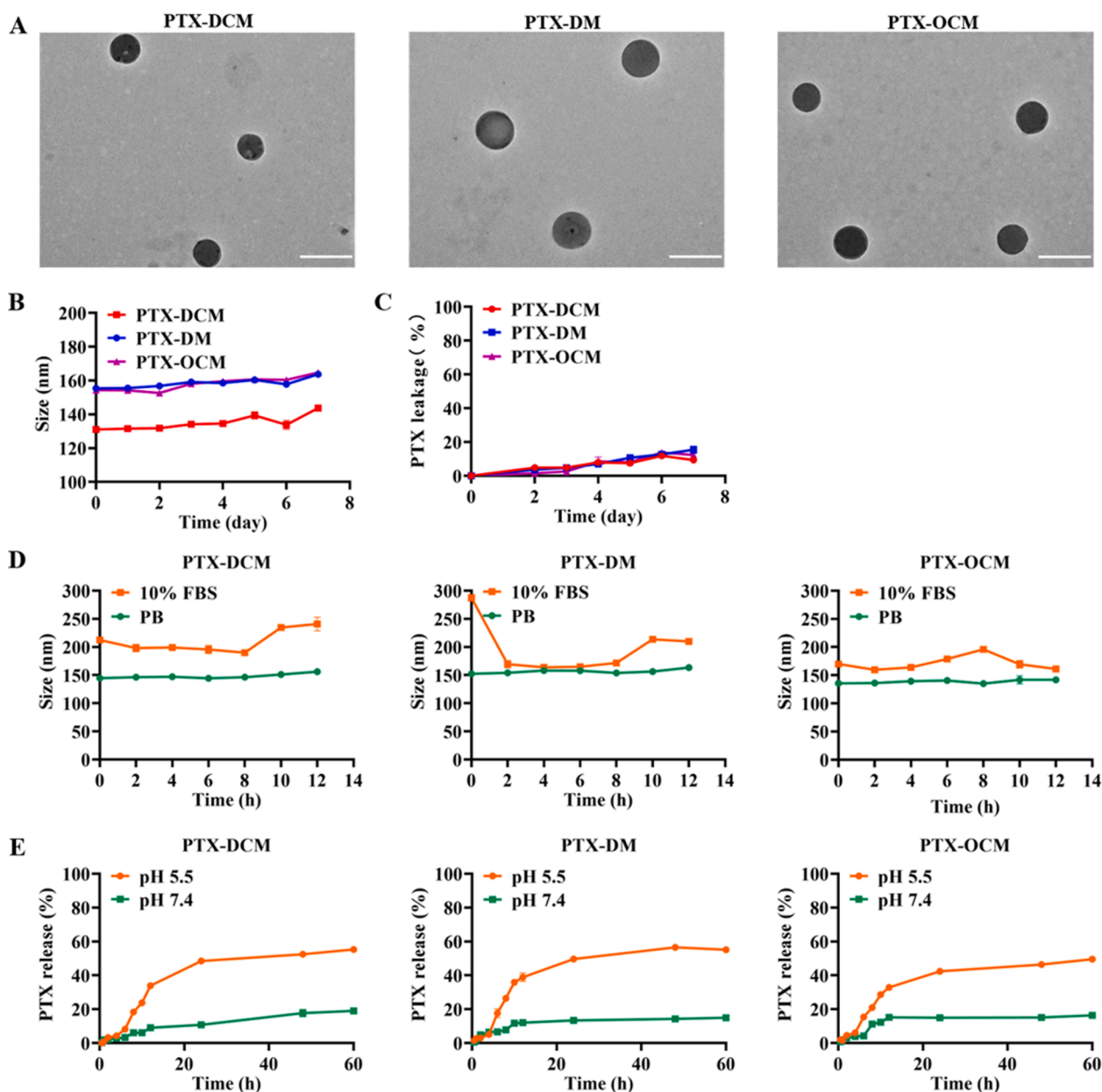


Fig. 4. Characterization of PTX-loaded micelles. (A) TEM images of various micelles. Scale bar: 200 nm. (B) Size changes and (C) drug leakage of various micelles at 4 °C within 7 days. (D) Size changes of various micelles in PB (pH 7.4) and DMEM containing 10% FBS at 37 °C during 12 h. (E) Accumulative PTX release from various micelles at pH 7.4 and pH 5.5 till 60 h. Data represented as mean ± SD, n = 3.

of potential drug vectors. Taken together, the chitosan derivatives prepared by the modular strategy possessed the comparable self-assemble ability, drug loading ability, and stability compared to the direct synthesis.

3.3. *In vitro* drug release

To realize an ideal treatment efficacy, chitosan-based micelles need to remain intact as much as possible during blood circulation but release drugs rapidly near the acidic environment of tumor sites. As depicted in Fig. 4E, PTX-DCM, PTX-DM, and PTX-OCM showed similar PTX release profiles at two different pH values. Less than 20% of PTX was released from chitosan micelles at pH 7.4 after 60 h, whereas the cumulative release surged to ~60% with the pH decreased to 5.5, suggesting a pH-dependent release characteristic for various PTX-loaded micelles. The pH-dependent release of various PTX-loaded micelles was probably ascribed to the protonation of sulfonate and primary amine groups at pH 5.5 which might disturb the stability of micelles, leading to the rapid release of PTX. These results hinted that module-synthesized chitosan derivatives could also be used as drug delivery carriers like the direct-synthesized counterparts.

3.4. *In vitro* safety assay

The safety of biomaterials directly determines their application prospects and is one of the core indicators for evaluating the practicability. In view of that the micelles assembled by DCSC, DSC, and OCSC have favorable performance in pharmaceutical studies, we in this part investigated the potential cytotoxicity against HUVEC cells by MTT assay. As illustrated in Fig. 5A, the 72 h-treatment with DCSC, DSC, and OCSC did not result in obvious antiproliferation even the concentrations were beyond 200 $\mu\text{g}/\text{mL}$, suggesting an acceptable safety towards HUVEC cells.

3.5. Cellular uptake

To explore the detailed cellular uptake of different micelles, the C6

fluorescence of MCF-7 cells was detected using CLSM and flow cytometry after incubation with C6-DCM, C6-DM, and C6-OCM from 0.5 h to 6 h, respectively. As shown in Fig. 5B-C, S6 and S7, the intracellular green fluorescence of all the C6-loaded micelles increased over time and gradually reached the peak at 4 h, which exhibited the consistent trend of internalization detected by flow cytometry and fluorescence images. In addition, we did not observe an obvious difference among the three micelles.

3.6. *In vitro* anticancer effect

The antiproliferative effect of PTX-loaded micelles against MCF-7 cells was evaluated utilizing the MTT assay, with Taxol® as a control. As exhibited in Fig. 6A, PTX-DCM, PTX-DM, and PTX-OCM presented concentration-dependent *in vitro* antitumor activity, and the IC_{50} values were calculated to be 1.19, 1.58, and 1.23 $\mu\text{g}/\text{mL}$, respectively (Fig. 6B). By comparison, the IC_{50} value of Taxol® was only 0.33 $\mu\text{g}/\text{mL}$, which was significantly lower than that of various PTX-loaded micelles. As for the reduced antiproliferative activity, it is ascribed to the slow release of PTX after being packaged into micelles.

4. Discussion

In this study, we described a modular strategy based on copper-free click reaction to synthesize amphiphilic chitosan derivatives including DCSC and OCSC, while the derivatives (DSC and OSC) with the same substitute groups and similar substitute degrees were synthesized using the direct synthesis of *N*-deoxychoylation or *N*-octanoylation as controls.

As we expected, the modular strategy can be successfully applied in the synthesis of chitosan derivatives with several advantages (Table 3). First, the modular strategy based on SPAAC reaction allows for simple mixture and stirring of raw materials at room temperature to afford the expected product, whereas direct amide coupling synthesis often needs other additive agents or heating. For example, EDCI/NHS is indispensable to catalyze amide couplings between SC and deoxycholic acid or octanoic acid, or the direct condensation does not work (Sperry et al.,

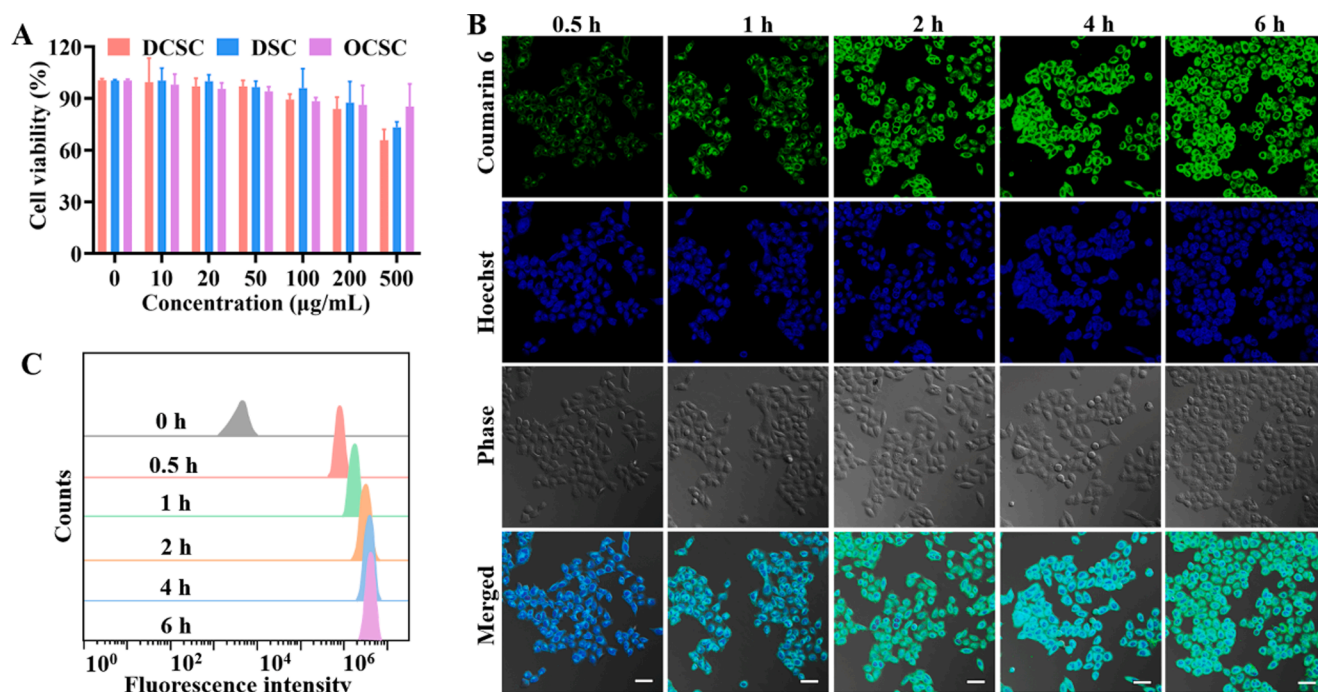


Fig. 5. Cellular evaluation. (A) *In vitro* cytotoxicity of various formulations against HUVEC cells. Data represented as mean \pm SD, $n = 3$. (B) Fluorescence images of C6-DCM accumulation in MCF-7 cells. Scale bar: 20 μm . (C) Representative flow cytometry diagrams of C6-DCM accumulation in MCF-7 cells.

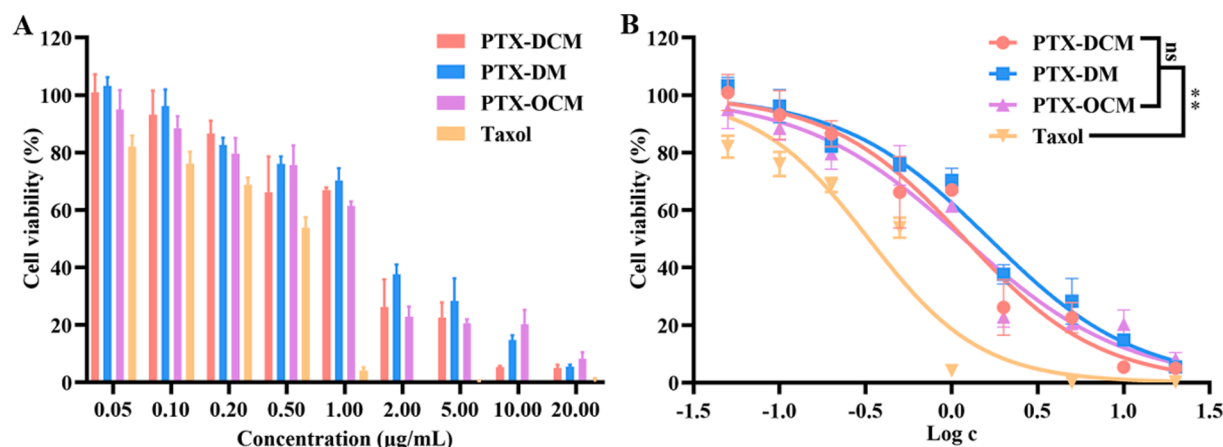


Fig. 6. (A) Antiproliferative effect of various PTX formulations at different concentrations against MCF-7 cells. $**P < 0.01$; data represented as mean \pm SD, $n = 3$. (B) IC₅₀ values of various PTX formulations. Data represented as mean \pm SD, $n = 3$.

Table 3

Comparison between modular and direct synthesis strategies.

	Modular strategy	Direct strategy
Reaction conditions	Gentle and simplified	Variable according to substituent groups
Reactivity	Highly efficient	Equivalence ratio raising to 7-fold
Yield	Higher than 90%	Lower than 70%
Reproducibility	High	Medium
Flexibility	Tolerance to a broad range of substrate scope	Limited to the specific reaction type and reactant
Environmental protection	No or harmful by-products	Poisonous impurities and additional pollution

2018). Second, the second-order rate constant of SPAAC reaction is as fast as $31.8 \text{ M}^{-1} \text{ s}^{-1}$, which means that the equivalence ratio of direct synthesis needs to increase by 7 times to achieve the similar graft ratio of modular strategy. Third, the modular strategy gives a remarkably high yield (up to 90%). Forth, the modular strategy shows the advantage of reproductivity due to the high reactivity and reaction controllability, which is of great importance to the pharmaceutical industry. Fifth, the modular strategy is more flexible than direct synthesis in regulating the substitution of various units as needed. Last but not the least, the modular strategy is eco-friendly because of the extremely high atom utilization with no or harmful by-products. Of note, the conjugation of ADIBO onto the chitosan provides π - π action with hydrophobic drugs, leading to an improvement in drug entrapment.

However, we have only adjusted the hydrophobic groups via the modular strategy in this study. The modification of other hydrophilic groups or functional groups such as the targeting ligands (Qindeel et al., 2019), pH-sensitive groups (Qu et al., 2020), ROS-sensitive groups (Liu et al., 2020), and so on can be attempted to confirm the advantages of modular strategy in synthesizing chitosan derivatives in future.

Moreover, the high drug loading ability and well biocompatibility of these chitosan-based micelles could be applied *in vivo* for the treatment of cancer. But the non-specific endocytosis of micelles might cause undesired side effects and reduce PTX accumulation at the tumor site. Therefore, targeting ligands like peptides, sugars or antibodies could be modified on chitosan micelles through SPAAC reaction to achieve active tumor targeting for effective tumor therapy.

5. Conclusion

In summary, we have successfully synthesized the chitosan derivatives of DCSC, OCSC, DSC, and OSC based on modular and direct amide coupling strategy, with the structure and physicochemical

properties estimated by multidimensional characterizations. PTX-loaded micelles assembled by DCSC, OCSC and DSC presented uniform particle sizes, negative zeta potentials, spherical morphology, good stability and acceptable biosafety, as well as high cytotoxicity against MCF-7 cells. Notably, the modular strategy held several advantages, including high reactivity and yield, flexibility, reproducibility, and eco-friendly ability. Taken together, SPAAC click chemistry-based modular synthesis is expected to act as a supplementary method for the preparation of multifunctional chitosan derivatives, which could provide varied chitosan derivatives in an easy and high-efficiency way and further improve the advancement of chitosan-based drug carriers.

CRedit authorship contribution statement

Yu Tao: Methodology, Validation, Writing - original draft. **Ding Qu:** Investigation, Formal analysis, Writing - review & editing. **Chunli Tian:** Conceptualization, Methodology, Validation. **Yingshuang Huang:** Software, Methodology. **Lingjing Xue:** Writing - review & editing. **Caoyun Ju:** Conceptualization, Supervision, Methodology, Writing - review & editing, Funding acquisition. **Meixi Hao:** Supervision, Methodology, Funding acquisition. **Can Zhang:** Supervision, Funding acquisition, Project administration.

Declaration of Competing Interest

The authors declare that they have no known competing financial interests or personal relationships that could have appeared to influence the work reported in this paper.

Acknowledgements

This work was supported by the National Natural Science Foundation of China (81930099, 81773664, 81473153, 82073785), National Major Scientific and Technological Special Project for "Significant New Drugs Development" (2019ZX09301163), the Natural Science Foundation of Jiangsu Province (BK20190558), 111 Project from the Ministry of Education of China and the State Administration of Foreign Expert Affairs of China (No. 111-2-07, B17047), the Open Project of State Key Laboratory of Natural Medicines (No. SKLNMZZ202017), and "Double First-Class" University project (CPU2018GY47, CPU2018GF10).

Appendix A. Supplementary material

Supplementary data to this article can be found online at <https://doi.org/10.1016/j.ijpharm.2021.120798>.

References

- Ali, A., Ahmed, S., 2018. A review on chitosan and its nanocomposites in drug delivery. *Int. J. Biol. Macromol.* 109, 273–286. <https://doi.org/10.1016/j.ijbiomac.2017.12.078>.
- Anselmo, A.C., Mitragotri, S., 2019. Nanoparticles in the clinic: an update. *Bioeng. Transl. Med.* 4 (3) <https://doi.org/10.1002/btm2.10143>.
- Becer, C.R., Hoogenboom, R., Schubert, U.S., 2009. Click chemistry beyond metal-catalyzed cycloaddition. *Angew. Chem. Int. Ed.* 48 (27), 4900–4908. <https://doi.org/10.1002/anie.200900755>.
- Campelo, C.S., Lima, L.D., Rebêlo, L.M., Mantovani, D., Beppu, M.M., Vieira, R.S., 2016. In vitro evaluation of anti-calcification and anti-coagulation on sulfonated chitosan and carrageenan surfaces. *Mater. Sci. Eng. C Mater. Biol. Appl.* 59, 241–248. <https://doi.org/10.1016/j.msec.2015.10.020>.
- Davis, M.E., Chen, Z., Shin, D.M., 2008. Nanoparticle therapeutics: an emerging treatment modality for cancer. *Nat. Rev. Drug Discov.* 7 (9), 771–782. <https://doi.org/10.1038/nrd2614>.
- de Oliveira Pedro, R., Schmitt, C.C., Neumann, M.G., 2016. Syntheses and characterization of amphiphilic quaternary ammonium chitosan derivatives. *Carbohydr. Polym.* 147, 97–103. <https://doi.org/10.1016/j.carbpol.2016.03.083>.
- Di Martino, A., Sedlarik, V., 2014. Amphiphilic chitosan-grafted-functionalized polylactic acid based nanoparticles as a delivery system for doxorubicin and temozolomide co-therapy. *Int. J. Pharmaceut.* 474 (1–2), 134–145. <https://doi.org/10.1016/j.ijpharm.2014.08.014>.
- Dimassi, S., Tabary, N., Chai, F., Blanchemain, N., Martel, B., 2018. Sulfonated and sulfated chitosan derivatives for biomedical applications: a review. *Carbohydr. Polym.* 202, 382–396. <https://doi.org/10.1016/j.carbpol.2018.09.011>.
- dos Santos, Z.M., Caroni, A.L.P.F., Pereira, M.R., da Silva, D.R., Fonseca, J.L.C., 2009. Determination of deacetylation degree of chitosan: a comparison between conductometric titration and CHN elemental analysis. *Carbohydr. Res.* 344 (18), 2591–2595. <https://doi.org/10.1016/j.carres.2009.08.030>.
- Du, H., Yang, X., Pang, X., Zhai, G., 2014. The synthesis, self-assembling, and biocompatibility of a novel O-carboxymethyl chitosan cholate decorated with glycyrrhetic acid. *Carbohydr. Polym.* 111, 753–761. <https://doi.org/10.1016/j.carbpol.2014.04.095>.
- Gabriel, J.S., Gonzaga, V.A.M., Poli, A.L., Schmitt, C.C., 2017. Photochemical synthesis of silver nanoparticles on chitosans/montmorillonite nanocomposite films and antibacterial activity. *Carbohydr. Polym.* 171, 202–210. <https://doi.org/10.1016/j.carbpol.2017.05.021>.
- Guo, X., Wei, X., Chen, Z., Zhang, X., Yang, G., Zhou, S., 2020. Multifunctional nanoplatfoms for subcellular delivery of drugs in cancer therapy. *Prog. Mater. Sci.* 107 <https://doi.org/10.1016/j.pmatsci.2019.100599>.
- Hashidzume, A., Nakamura, T., Sato, T., 2013. Copper-catalyzed azide-alkyne cycloaddition oligomerization of 3-azido-1-propyne derivatives. *Polymer* 54 (14), 3448–3451. <https://doi.org/10.1016/j.polymer.2013.05.010>.
- Jin, X., Mo, R., Ding, Y., Zheng, W., Zhang, C., 2014. Paclitaxel-loaded N-octyl-O-sulfate chitosan micelles for superior cancer therapeutic efficacy and overcoming drug resistance. *Mol. Pharm.* 11 (1), 145–157. <https://doi.org/10.1021/mp400340k>.
- Jung, S., Yi, H., 2013. Facile strategy for protein conjugation with chitosan-poly(ethylene glycol) hybrid microparticle platforms via strain-promoted alkyne-azide cycloaddition (SPAAC) reaction. *Biomacromolecules* 14 (11), 3892–3902. <https://doi.org/10.1021/bm401018h>.
- Kim, Y.H., Gihm, S.H., Park, C.R., Lee, K.Y., Kim, T.W., Kwon, I.C., Chung, H., Jeong, S. Y., 2001. Structural characteristics of size-controlled self-aggregates of deoxycholic acid-modified chitosan and their application as a DNA delivery carrier. *Bioconjug. Chem.* 12 (6), 932–938. <https://doi.org/10.1021/bc015510c>.
- Kuzmin, A., Poloukhina, A., Wolfert, M.A., Popik, V.V., 2010. Surface functionalization using catalyst-free azide-alkyne cycloaddition. *Bioconjug. Chem.* 21 (11), 2076–2085. <https://doi.org/10.1021/bc100306u>.
- Lai, M., Wang, J., Tan, J., Luo, J., Zhang, L.M., Deng, D.Y., Yang, L., 2017. Preparation, complexation mechanism and properties of nano-complexes of Astragalus polysaccharide and amphiphilic chitosan derivatives. *Carbohydr. Polym.* 161, 261–269. <https://doi.org/10.1016/j.carbpol.2016.12.068>.
- Lee, D.E., Na, J.H., Lee, S., Kang, C.M., Kim, H.N., Han, S.J., Kim, H., Choe, Y.S., Jung, K. H., Lee, K.C., Choi, K., Kwon, I.C., Jeong, S.Y., Lee, K.H., Kim, K., 2013. Facile method to radiolabel glycol chitosan nanoparticles with (64)Cu via copper-free click chemistry for MicroPET imaging. *Mol. Pharm.* 10 (6), 2190–2198. <https://doi.org/10.1021/mp300601r>.
- Liu, D., Shu, G., Jin, F., Qi, J., Xu, X., Du, Y., Yu, H., Wang, J., Sun, M., You, Y., Zhu, M., Chen, M., Zhu, L., Shen, Q., Ying, X., Lou, X., Jiang, S., Du, Y., 2020. ROS-responsive chitosan-SS31 prodrug for AKI therapy via rapid distribution in the kidney and long-term retention in the renal tubule. *Sci. Adv.* 6 (41), eabb7422. <https://doi.org/10.1126/sciadv.abb7422>.
- Mo, R., Xiao, Y., Sun, M., Zhang, C., Ping, Q., 2011. Enhancing effect of N-octyl-O-sulfate chitosan on etoposide absorption. *Int. J. Pharm.* 409 (1), 38–45. <https://doi.org/10.1016/j.ijpharm.2011.02.021>.
- Qindeel, M., Ahmed, N., Khan, G.M., Rehman, A.U., 2019. Ligand decorated chitosan as an advanced nanocarrier for targeted delivery: a critical review. *Nanomedicine (Lond.)* 14 (12), 1623–1642. <https://doi.org/10.2217/nmm-2018-0490>.
- Qu, D., Jiao, M., Lin, H., Tian, C., Qu, G., Xue, J., Xue, L., Ju, C., Zhang, C., 2020. Anisamide-functionalized pH-responsive amphiphilic chitosan-based paclitaxel micelles for sigma-1 receptor targeted prostate cancer treatment. *Carbohydr. Polym.* 229 <https://doi.org/10.1016/j.carbpol.2019.115498>.
- Qu, D., Lin, H., Zhang, N., Xue, J., Zhang, C., 2013. In vitro evaluation on novel modified chitosan for targeted antitumor drug delivery. *Carbohydr. Polym.* 92 (1), 545–554. <https://doi.org/10.1016/j.carbpol.2012.08.112>.
- Seedevi, P., Moovendhan, M., Vairamani, S., Shanmugam, A., 2017. Evaluation of antioxidant activities and chemical analysis of sulfated chitosan from Sepia prashadi. *Int. J. Biol. Macromol.* 99 (Suppl. C), 519–529. <https://doi.org/10.1016/j.ijbiomac.2017.03.012>.
- Smyslova, P., Popa, I., Lycka, A., Tejral, G., Hlavac, J., 2015. Non-catalyzed click reactions of ADIBO derivatives with 5-methyluridine azides and conformational study of the resulting triazoles. *PLoS ONE* 10 (12). <https://doi.org/10.1371/journal.pone.0144613>.
- Hawksworth, M., Oke, S., Richardson, P.F., Barnhart, R., Bill, D.R., Giusto, R.A., Weaver, J.D., 2018. Thermal stability assessment of peptide coupling reagents commonly used in pharmaceutical manufacturing. *Org. Process Res. Dev.* 22 (9), 1262–1275. <https://doi.org/10.1021/acs.oprd.8b00193>.
- Sun, T., Zhou, D., Mao, F., Zhu, Y., 2007. Preparation of low-molecular-weight carboxymethyl chitosan and their superoxide anion scavenging activity. *Eur. Polym. J.* 43 (2), 652–656. <https://doi.org/10.1016/j.eurpolymj.2006.11.014>.
- Wakita, M.A., 2013. Removal of lipopolysaccharide from protein solution using nanostructured porous supports bearing lipid membranes. *Nanoscale Res. Lett.* 8 (1), 460. <https://doi.org/10.1186/1556-276X-8-460>.
- Wang, X., Li, Z., Shi, T., Zhao, P., An, K., Lin, C., Liu, H., 2017. Injectable dextran hydrogels fabricated by metal-free click chemistry for cartilage tissue engineering. *Mater. Sci. Eng. C Mater. Biol. Appl.* 73, 21–30. <https://doi.org/10.1016/j.msec.2016.12.053>.
- Wu, C., Tian, J., Li, S., Wu, T., Hu, Y., Chen, S., Sugawara, T., Ye, X., 2016. Structural properties of films and rheology of film-forming solutions of chitosan gallate for food packaging. *Carbohydr. Polym.* 146, 10–19. <https://doi.org/10.1016/j.carbpol.2016.03.027>.
- Yu, X., Mu, Y., Xu, M., Xia, G., Wang, J., Liu, Y., Chen, X., 2017. Preparation and characterization of mucosal adhesive and two-step drug releasing cetirizine-chitosan nanoparticle. *Carbohydr. Polym.* 173, 600–609. <https://doi.org/10.1016/j.carbpol.2017.05.067>.
- Zhang, N., Xu, X., Zhang, X., Qu, D., Xue, L., Mo, R., Zhang, C., 2016. Nanocomposite hydrogel incorporating gold nanorods and paclitaxel-loaded chitosan micelles for combination photothermal-chemotherapy. *Int. J. Pharm.* 497 (1), 210–221. <https://doi.org/10.1016/j.ijpharm.2015.11.032>.
- Zou, Y., Zhang, L., Yang, L., Zhu, F., Ding, M., Lin, F., Wang, Z., Li, Y., 2018. “Click” chemistry in polymeric scaffolds: bioactive materials for tissue engineering. *J. Control. Release* 273, 160–179. <https://doi.org/10.1016/j.jconrel.2018.01.023>.